Benchmarkings for a semiclassical impurity solver for dynamical-mean-field theory: Self-energies and magnetic transitions of the single-orbital Hubbard model

Satoshi Okamoto,[1,*] Andreas Fuhrmann,[2] Armin Comanac,[1] and Andrew J. Millis[1]
[1]*Department of Physics, Columbia University, 538 West 120th Street, New York, New York 10027, USA*
[2]*Physikalisches Institut, Universität Bonn, Nußallee 12, D-53115 Bonn, Germany*
(Received 1 February 2005; published 24 June 2005)

An investigation is presented of the utility of semiclassical approximations for solving the quantum-impurity problems arising in the dynamical-mean-field approach to correlated-electron models. The method is based on performing an exact numerical integral over the zero-Matsubara-frequency component of the spin part of a continuous Hubbard-Stratonovich field, along with a spin-field-dependent steepest descent treatment of the charge part. We test this method by applying it to one- or two-site approximations to the single-band Hubbard model with different band structures, and comparing the results to quantum Monte Carlo and simplified exact diagonalization calculations. The resulting electron self-energies, densities of states, and magnetic transition temperatures show reasonable agreement with the quantum Monte Carlo simulation over wide parameter ranges, suggesting that the semiclassical method is useful for obtaining a reasonable picture of the physics in situations where other techniques are too expensive.

DOI: 10.1103/PhysRevB.71.235113 PACS number(s): 71.10.Fd, 75.10.−b

I. INTRODUCTION

Correlated-electron materials, in which the interaction energy is comparable to or larger than the electron kinetic energy, are an important topic in materials science. In these compounds, standard band theory is an inadequate representation of the physics. The discovery of high-T_c superconductivity in the oxide cuprates[1] led to greatly increased interest in correlated-electron compounds. Many materials have been studied, and many novel properties have been discovered, including colossal magnetoresistance, variety of spin, orbital, charge orderings, and unconventional superconductivity.[2,3] Understanding the novel phenomena and determining the correct electronic phases in these materials are challenging tasks, and are indispensable for developing electronic devices exploiting these properties of correlated-electron materials. However, the rapid increase of Hilbert space with system size limits the utility of exact-diagonalizaion (ED) methods, while the fermion "sign problem" renders Monte Carlo (MC) approaches ineffective.

Dynamical-mean-field theory (DMFT) is a promising approach for treating correlation effects.[4–6] The method may be combined with realistic band-structure calculations, and has been applied to a variety of materials (see Refs. 7–10 for example). In DMFT, the momentum-dependent electron self-energy is approximated as a finite set of functions of frequency, and the physical lattice problem is mapped into one or several coupled impurity-Anderson models (IAMs) with the environment determined self-consistently. To solve the IAM, a variety of theoretical methods have been applied, including analytical approximations such as iterated perturbation theory,[6,11–13] the noncrossing approximation,[14] the projective self-consistent method,[15] and the slave-boson method,[16] for example, and numerical methods including quantum Monte Carlo (QMC),[17–19] exact diagonalization,[20] numerical renormalization group,[21,22] and density-matrix renormalization group.[23,24] Most interesting phenomena cannot be addressed by analytical methods. Numerical methods, however, are computationally very expensive. In order to combine DMFT with a realistic band-structure calculation and survey a wide range of parameters, it is desirable to develop computationally cheap and reliable methods. Methods that can reproduce the correct electronic phases and distinguish phases near in energy at low temperature are particularly needed. Many ideas have been proposed to reduce the computational cost.[25–30] These fall mainly into two groups: approximating the environment by a small finite number of orbitals,[25,26] and perturbative methods involving expansions around a certain solvable limit.[27–30] The approximated-environment methods provide a good approximation to the $T=0$ Mott physics of the Hubbard model;[25,26] however, because only a small number of states are used, it has difficulty dealing with the thermodynamics (as discussed later), and becomes impractical for multiorbital and multisite systems. Perturbative methods are not reliable at intermediate coupling. Nonperturbative methods which can deal with the thermodynamics are required.

In this paper, we investigate an alternative method to solve the IAM in DMFT formalism: a semiclassical approximation based on the continuous Hubbard-Stratonovich transformation.[31] This method is computationally very cheap (approximately two orders of magnitude faster than the QMC technique for single-impurity models, and with a better scaling with system size): it may be performed on a commercial PC. The semiclassical approximation, in the form used here, was apparently first proposed by Hasegawa,[32] who used it to study a "single-site spin fluctuation theory" which may be viewed as an early, simplified version of dynamical-mean-field theory. Semiclassical methods were also used by Blawid and Millis[33] and by Pankov, Kotliar, and Motome[34] to study models of electrons coupled to large-mass oscillators. In this paper, we present an implementation in the context of dynamical-mean-field theory, and test its reliability for a fully quantal model problem, namely, the Hubbard model on

a variety of lattices by performing detailed comparisons between the semiclassical approximation and a QMC calculation. We also present a brief comparison to a successful "truncated-environment method:" the two-site DMFT.[25] The semiclassical approximation is found to be reasonable at high temperature and in the strong coupling regime, and gives good results for magnetic transitions. In the half-filled square lattice, the Néel temperature computed by the semiclassical approximation is very close to that found in QMC simulations. In the metallic face-centered cubic (fcc) lattice, ferromagnetic Curie temperatures computed by the present method are within a factor of 2 compared with the QMC results, and the competition between ferro- and antiferromagnetism is correctly captured; $T=0$ phase boundaries are obtained within an error of $\sim 20\%$ compared to QMC results. The $T=0$ phase boundaries are in the same range as found in two-site DMFT, but this latter method gives very poor transition temperatures. We also use the semiclassical approximation to compute dynamical properties, in particular, the electron self-energy and spectral functions, which are found to be in reasonable agreement with QMC results.

The rest of this paper is organized as follows. Section II formulates the semiclassical approximation. In Sec. III, we use the Gaussian fluctuation approximation to estimate the limits of validity of the semiclassical approximation. Sections IV and V compare numerical results for the semiclassical approximation to QMC, ED, and Hartree-Fock (HF) results, for the single-band Hubbard model on a square lattice and a face-centered cubic lattice, respectively. Section VI presents an application of the method to the two-impurity cluster dynamical-mean-field approximation for the half-filled Hubbard model. Comparison of nearest-neighbor spin correlation between the semiclassical approximation and the QMC method are given. In Sec. VII, we discuss the equilibration problem associated with the partitioned phase space in the semiclassical approximation and QMC simulation. Finally, Sec. VIII gives a summary and discussion.

II. FORMULATION

In this section, we derive the semiclassical approximation from the continuous Hubbard-Stratonovich (HS) transformation.[31] We consider a single-orbital repulsive Hubbard model for simplicity: $H=H_{band}+H_U$ with H_{band} and H_U being the single-particle dispersion and interaction terms, respectively. Generalizations to multiorbital and long-range interaction would also be possible: see, e.g., Refs. 35–39.

We take the band-dispersion term to be $H_{band}=\Sigma_{k\sigma}\varepsilon_k c^\dagger_{k\sigma}c_{k\sigma}$ with three choices of ε_k.

On the two-dimensional square lattice,

$$\varepsilon_{\vec{k}}^{square} = -2t(\cos k_x + \cos k_y). \tag{1}$$

On the three-dimensional fcc lattice,

$$\varepsilon_{\vec{k}}^{fcc3} = 4t(\cos k_x \cos k_y + \cos k_y \cos k_z + \cos k_z \cos k_x) + 2t'(\cos 2k_x + \cos 2k_y + \cos 2k_z), \tag{2}$$

where t and t' are the nearest-neighbor (NN) and the second NN hopping, respectively.

On the infinite-dimensional fcc lattice, the noninteracting density of states is given by

$$N^{fcc\infty}(\varepsilon) = \frac{\exp\{-(1+\sqrt{2}\varepsilon)/2\}}{\sqrt{\pi(1+\sqrt{2}\varepsilon)}}, \tag{3}$$

which diverges at the bottom of the band. $N^{fcc\infty}$ was introduced by Müller-Hartmann[42] and studied in detail by Ulmke.[43] Here, energy is scaled by the variance of the density of states (DOS) ($v=1$). The fcc lattices are of interest because these display a ferromagnetic phase in a wide range of doping.

The interaction term is given by

$$H_U = U\sum_i n_{i\uparrow}n_{i\downarrow} \tag{4}$$

with $U>0$.

In the DMFT approximation, one first needs to compute the partition function of an N-site impurity model as

$$Z = \int \mathcal{D}[c^\dagger, c]\exp\{-(\mathcal{S}_0 + \mathcal{S}_{int})\}, \tag{5}$$

with

$$\mathcal{S}_0 = -\int_0^\beta d\tau\, d\tau'\, \psi^\dagger_\sigma(\tau)\mathbf{a}_\sigma(\tau-\tau')\psi_\sigma(\tau') \tag{6}$$

where $\psi=[c_1,\ldots,c_N]^t$ with c_i ($c_i^\dagger$) being a Grassmann number corresponding to the electron annihilation (creation) operator at site i. $\mathbf{a}_\sigma$ is the $N\times N$ matrix Weiss field (inverse of the noninteracting Green's function) which will be determined self-consistently, and $\beta=1/T$ is the inverse temperature. $\mathcal{S}_{int}$ represents the interaction term specified by the model one considers. For the single-band Hubbard model, $\mathcal{S}_{int}=U\int d\tau \Sigma_i n_{i\uparrow}(\tau)n_{i\downarrow}(\tau)$.

Next, one computes the single-particle interacting Green's function $\mathbf{G}_\sigma$ by a functional derivative of $\ln Z$ with respect to $\mathbf{a}_\sigma$ as

$$\mathbf{G}_\sigma = \frac{\delta \ln Z}{\delta \mathbf{a}_\sigma}. \tag{7}$$

The electronic self-energy is obtained by inverting the Dyson equation as

$$\mathbf{\Sigma}_\sigma = \mathbf{a}_\sigma - \mathbf{G}_\sigma^{-1}. \tag{8}$$

Finally, by connecting the impurity Green's function $\mathbf{G}$ and the local part of the lattice Green's function, the DMFT equation is closed. The self-consistency equation for the ij component of $\mathbf{G}$ is

$$G_{ij\sigma}(i\omega_n) = \int \left(\frac{dk}{2\pi}\right)^d \left[\frac{\varphi_{ij}(k)}{i\omega_n + \mu - \mathbf{t}_k - \mathbf{\Sigma}_{k\sigma}(i\omega_n)}\right]_{ij}, \tag{9}$$

where ω_n is the fermionic Matsubara frequency, and $\mathbf{t}_k$ and $\mathbf{\Sigma}_k$ are the Fourier transforms of the hopping and the self-energy matrices, respectively. $\varphi_{ij}(k)$ is a form factor specified by the DMFT method chosen.[40] The chemical potential μ is fixed so that $\mathbf{G}$ gives the correct electron density n. The local Green function $\mathbf{G}$ is used to update the Weiss field $\mathbf{a}_\sigma^{new}$ as

$\mathbf{a}_\sigma^{new}=\mathbf{G}_\sigma^{-1}+\mathbf{\Sigma}_\sigma$, and this process is repeated until the self-consistency $\mathbf{a}_\sigma=\mathbf{a}_\sigma^{new}$ is obtained. The expensive computational task is evaluating the functional integral in Eq. (5).

A key point of the present approximation for the single-band Hubbard model is introducing the charge field as well as spin. Using the following identity:

$$n_\uparrow n_\downarrow = \frac{1}{4}(\rho^2 - m^2), \tag{10}$$

with $\rho=n_\uparrow+n_\downarrow$ and $m=n_\uparrow-n_\downarrow$, we perform the HS transformation $\exp(-\mathcal{S}_{int})=\int\mathcal{D}[\varphi,x]\exp(-\mathcal{S}'_{int})$ with the effective interaction

$$\mathcal{S}'_{int} = \frac{1}{4U}\int_0^\beta d\tau\Bigg(\{\varphi^2(\tau)+x^2(\tau)\} - 2U\sum_\sigma c_\sigma^\dagger(\tau)\{\varphi(\tau)\sigma_z + ix(\tau)\}c_\sigma(\tau)\Bigg), \tag{11}$$

where φ and x are the HS fields acting on spin and charge degrees of freedom, respectively, and σ_z is the z component of the Pauli matrices. Now, one can perform the Grassmann integral over the fermionic field formally to obtain the partition function

$$Z = \int \mathcal{D}[\varphi,x]\exp(-\mathcal{S}_{eff}) \tag{12}$$

with the effective action

$$\mathcal{S}_{eff} = \frac{1}{4U}\int_0^\beta d\tau\{\varphi^2(\tau)+x^2(\tau)\} - \mathrm{Tr}\ln\left(-a_\sigma - \frac{1}{2}(\varphi\sigma_z + ix)\right). \tag{13}$$

Here, the trace includes spin as well as Matsubara frequency. It is noted that the coupling constant for the charge field x is imaginary. This originates from the different sign of quadratic terms for spin and charge when decoupling the interaction term [see Eq. (10)].

Exact evaluation of the partition function Eq. (12) is impossible. The simplest approximation is to approximate the integrals by the value computed using the static parts $\bar{\varphi}$ and $\bar{x}$ which minimize the action [solutions of the saddle-point equations $\partial\mathcal{S}(\bar{\varphi},\bar{x})/\partial\bar{\varphi}=\partial\mathcal{S}(\bar{\varphi},\bar{x})/\partial\bar{x}=0$]. This is the Hartree-Fock approximation, which is known to give a poor estimate for transition temperatures and self-energies. One may correct the HF approximation by including the Gaussian fluctuations in which $\mathcal{S}_{eff}$ is expanded around the saddle point up to the quadratic order of the fluctuations $\delta\varphi(\tau)$ and $\delta x(\tau)$. In this case, $\delta\varphi(\tau)$ and $\delta x(\tau)$ decouple. However, Gaussian fluctuation theory is limited to the weak coupling regime. As an example, Fig. 1 shows an effective potential V for φ, equivalent to $T\mathcal{S}_{eff}$, calculated (as explained below) by the semiclassical approximation. It is seen that the potential is highly nonparabolic, and the variation in V is on the scale of T for reasonable T. Thus, the Gaussian fluctuation theory is inapplicable. Next, one can consider taking φ and x only at the Matsubara frequency $\nu_l=0$, i.e., the static approximation, but evaluating the partition function Z as a two-dimensional integral over two static fields (two-field approximation). The partition function is expressed as $Z_{static}=\int d\varphi\, dx\exp(-\mathcal{S}_{static})$ with

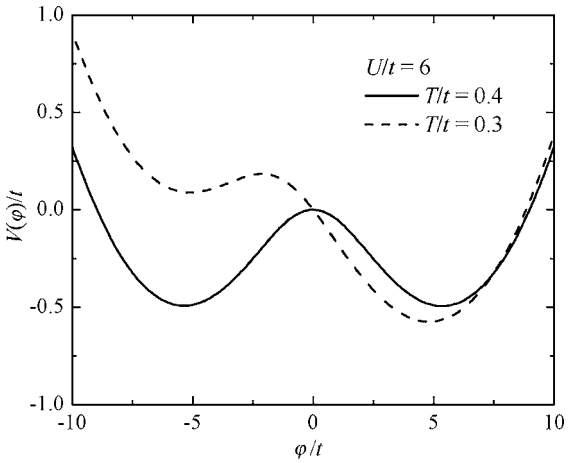

FIG. 1. Example of the effective potential for φ, $V(\varphi)$ given in Eq. (16), in the square-lattice half-filled Hubbard model with $U/t=6$. Solid line, $T/t=0.4$ (about 14% above $T_N\sim 0.35t$); broken line, $T/t=0.3$ (about 14% below T_N). At both temperatures, V is far from a simple parabola, and regions far from the local minima have appreciable occupation probability.

$$\mathcal{S}_{static} = \frac{\beta}{4U}(\varphi^2+x^2) - \mathrm{Tr}\ln\left(-a_\sigma - \frac{1}{2}(\varphi\sigma_z + ix)\right). \tag{14}$$

However, this approximation fails because the effective action $\mathcal{S}_{static}$ is complex and $\exp(-\mathcal{S}_{static})$ cannot be regarded as a distribution function of φ and x, leading to poor convergence of integrals. With some effort, apparently converged integrals can be obtained, but the interacting Green's function computed by using Eq. (7) with Z replaced by Z_{static} does not behave correctly; the imaginary part of the self-energy changes sign and the spectral-function sum rule is strongly violated. As an example, Fig. 2 compares self-energies computed by evaluating the static average and integrating over two static fields φ and x with the action Eq. (14) to the semiclassical approximation defined shortly. While we have obtained a converged solution along the Matsubara axis, the imaginary part of the self-energy changes sign and causality is strongly violated, so that the analytic continuation to the real axis is impossible.

In order to reduce the above mentioned problems and to take into account the fluctuation of both fields to some extent, we apply the semiclassical approximation, following Hasegawa.[32] In this method, we first solve the mean-field equation for the static charge field $\bar{x}_\varphi$ which minimizes $\mathcal{S}$ at a given value of φ. From $\partial\mathcal{S}_{eff}/\partial\bar{x}|_\varphi=0$, we obtain the following equation ($\xi_\varphi=i\bar{x}|_\varphi$):

$$\xi_\varphi = -UT\,\mathrm{Tr}\frac{1}{a_\sigma + (\varphi\sigma_z+\xi_\varphi)/2}. \tag{15}$$

Here, Tr involves a convergency factor $e^{i\omega_n 0_+}$. By solving Eq. (15), one obtains ξ_φ as a function of φ. In the single-impurity model, this equation has a unique solution; thus, Eq. (15) can be solved easily, for example, via bisection. (For multi-

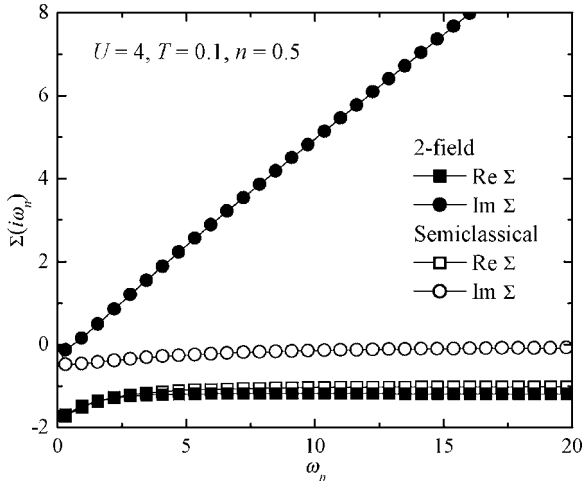

FIG. 2. Comparison of the electron self-energy computed by evaluating the static average and integrating over two static fields φ and x with the action Eq. (14) (2-field) and the semiclassical approximation, which is defined in this section, for the infinite-dimensional fcc lattice Eq. (3). Energy is scaled by the variance of the free DOS ($v=1$). Squares (circles) are real (imaginary) parts of the self-energy, and filled and open symbols are obtained by the two-field approximation and the semiclassical approximation, respectively.

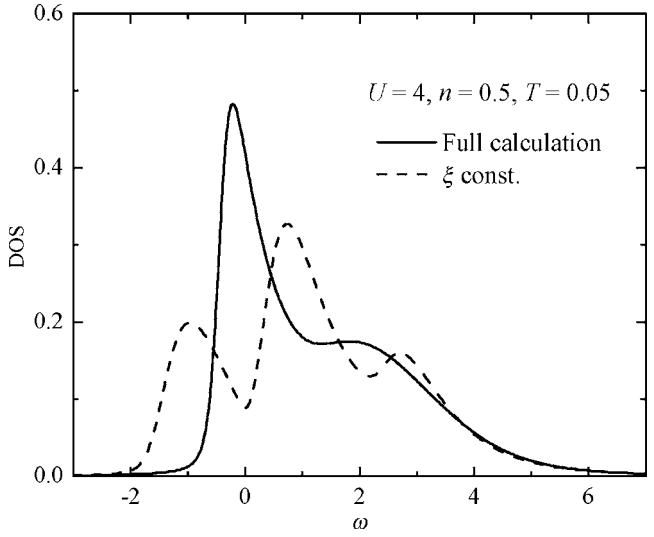

FIG. 3. Comparison of the many-body density of states computed for the paramagnetic phase of the infinite-dimensional fcc lattice [Eq. (3)] by the "full" semiclassical approximation (solid line) to that computed using an additional approximation in which ξ is assumed to be independent of φ (broken line). Energy is scaled by the variance of the free DOS ($v=1$). The three-peak structure seen in the broken line is unphysical; the solid line is in good agreement with QMC results (not shown). Note that $T_C \sim 0.073$ for these parameters; we have presented data at $T=0.05 \simeq 3T_C/4$ (chosen to reveal the three-peak structure clearly), and have artificially suppressed ferromagnetism.

impurity models, we have no proof that there is a unique solution, but difficulties have not arisen in the case we have studied.) Fluctuations of the charge field around this saddle point are expected to be less important than those of the spin field, because of the unique solution and because charge fluctuations are not soft, and the difficulties associated with the oscillatory convergence of Eq. (14) are avoided.

The φ dependence of ξ is crucial. If it is neglected, i.e., if ξ is taken to be the value ξ_{av} which minimizes S_{eff} after averaging over φ, then one obtains a model equivalent to the Jahn-Teller phonon model studied, for example, in Ref. 41. This latter model has different physics from the Hubbard model. In particular, the Jahn-Teller model has a spectral function with a characteristic three-peak structure quite unlike the spectral function of Hubbard-like models. An example of the density of states computed by the approximation $\xi_\varphi \to \xi_{av}$ is shown as the broken line in Fig. 3. One can clearly observe a three-peak structure. The outer two peaks correspond to the occupied (lower band) and unoccupied (upper band) state at the occupied distorted site (from a potential minima at $\varphi \sim \pm U$), and the middle peak corresponds to the unoccupied undistorted state (from a potential minimum at $\varphi \sim 0$) in the phonon model. In the phonon model, the level separation between the lower occupied state and the middle unoccupied one has physical meaning as "polaron binding," which does not exist in the original Hubbard model. The spectral function computed from the "full" semiclassical method (see below) is shown as the solid line in Fig. 3, and as will be seen below is in much better agreement with QMC data.

Now that the saddle point of the effective action is determined with respect to one of two variables, ξ, an effective potential for the remaining variable φ is written as

$$V(\varphi) = \frac{1}{4U}(\varphi^2 - \xi_\varphi^2) - T\,\mathrm{Tr}\,\ln\left(-a_\sigma - \frac{1}{2}(\varphi\sigma_z + \xi_\varphi)\right), \tag{16}$$

where Tr involves a convergency factor $e^{i\omega_n 0_+}$. With this effective potential, the partition function is approximated as

$$Z_{approx} = \int_{-\infty}^{\infty} d\varphi\, \exp\{-\beta V(\varphi)\}. \tag{17}$$

There remains only one variable φ, which is purely real. Numerical integrals can be performed without difficulty. Figure 4 shows an example of $V(\varphi)$ and ξ_φ calculated by the "full" semiclassical approximation for a noninteger filling. It is seen again that V is highly nonparabolic. Furthermore, ξ_φ depends on φ, indicating the strong coupling between spin and charge fields.

Now that the approximate partition function Z_{approx} is obtained, one can obtain the physical quantity from the functional derivative form following the DMFT procedure. The impurity Green's function is

$$G_\sigma = \frac{\delta \ln Z_{approx}}{\delta a_\sigma} = \left\langle \frac{1}{a_\sigma + (\varphi\sigma_z + \xi_\varphi)/2} \right\rangle, \tag{18}$$

where $\langle \cdots \rangle$ stands for $\int d\varphi\, \exp\{-\beta V(\varphi)\} \cdots / Z_{approx}$. Thus, Eqs. (15)–(18) with the DMFT self-consistency equation construct the present semiclassical approximation.

It may be useful to mention the correspondence between the present theory and the single-site spin-fluctuation theory

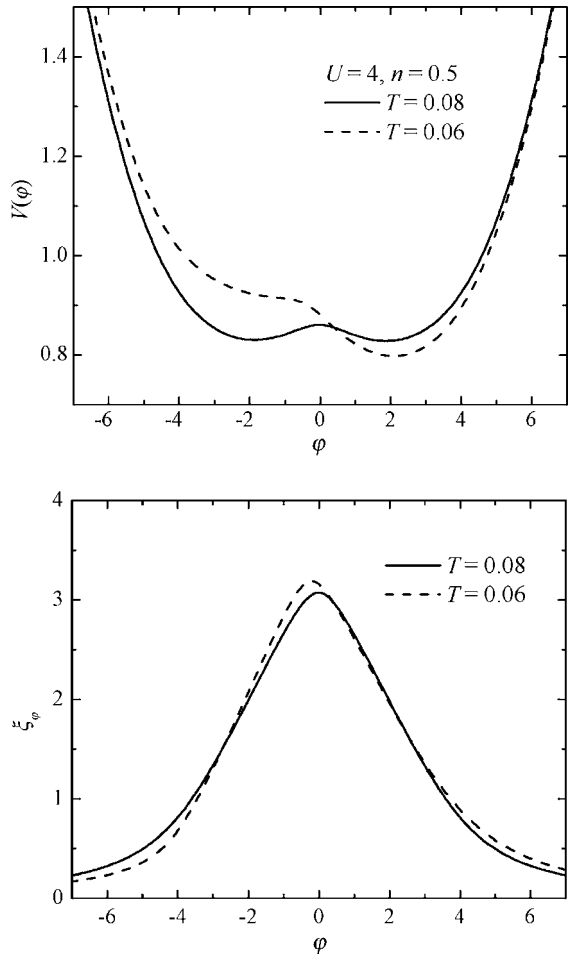

FIG. 4. Example of the effective potential V (upper panel) and charge field ξ as functions of φ in the metallic Hubbard model on an infinite-dimensional fcc lattice [the free DOS is given in Eq. (3)] with $U=4$ and $n=0.5$. Energy is scaled by the variance of free DOS ($v=1$). Solid lines, $T=0.08$ (about 14% above $T_C \sim 0.073$); broken lines, $T=0.06$ (about 18% below T_C). A constant term ($=-U$) has been subtracted from ξ. At both temperatures, the potential is seen to differ markedly from a simple parabola. The φ dependence of ξ indicates strong coupling between the two fields.

of Hasegawa.[32] In Ref. 32, Hasegawa introduced the same HS transformation using spin and charge fields, and applied the saddle-point approximation against the charge field. Thus, up to this point, the two theories are equivalent, but instead of Eq. (18) and the DMFT self-consistency equation, Hasegawa used an *ad hoc* procedure involving computation of averages of the magnetic moment and square of the magnetic moment.

We emphasize, however, that the semiclassical approximation is not exact. In weak coupling, it leads to a scattering rate proportional to T, rather than to T^2/E_F, and does not give a mass renormalization; in strong coupling, while it gives correct Mott insulator behavior, i.e., divergence of the on-site self-energy proportional to $1/(i\omega_n)$, the self-energy at small ω remains finite at $T \to 0$ even in a paramagnetic metallic phase as long as the effective potential $V(\varphi)$ has more than one degenerate minimum, implying incorrect non-Fermi-liquid behavior. This originates from the neglect of the quantum fluctuation of HS fields. Including the quantum fluctuation to recover the correct Fermi-liquid behavior is not easy.[34,45,46] Although, it is not exact, it will be shown below that the semiclassical method gives good estimates of the important physical quantities.

III. WEAK COUPLING GAUSSIAN APPROXIMATION: COMPARISON OF CLASSICAL AND EXACT RESULTS

This section uses the Gaussian approximation to the paramagnetic phase of the functional integral to gain insight into the limits of validity of the classical approximation. The advantage of the Gaussian approximation is that any desired quantity can be computed straightforwardly, permitting a detailed comparison of the results of the classical approximation to the fully quantal calculation. We consider the mean square amplitude of the spin Hubbard-Stratonovich field, $\langle \varphi^2 \rangle$, and also the Matsubara-axis electron self-energy $\sigma(i\omega_n)$.

In the Gaussian approximation one determines the values $\bar{\varphi} = UT \,\mathrm{Tr}_{\omega_n,\sigma} \sigma_z \left[a_0 + \frac{1}{2}(\bar{\varphi}\sigma_z + i\bar{x}) \right]^{-1}$ and $\bar{x} = iUT \,\mathrm{Tr}_{\omega_n,\sigma} \left[a_0 + \frac{1}{2}(\bar{\varphi}\sigma_z + i\bar{x}) \right]^{-1}$ which extremize the argument of the exponential, and then expand the argument of the exponential to second order in the deviations of the fields from their extremal values:

$$Z \to \bar{Z} \int \mathcal{D}[\varphi x] \exp\left[-S_\varphi^{(2)} - S_x^{(2)} \right], \tag{19}$$

where $\bar{Z}$ is the contribution from the saddle points, and

$$S_\lambda^{(2)} = \int d\tau_1 d\tau_2 \lambda(\tau_1) \chi_\lambda^{-1}(\tau_1 - \tau_2) \lambda(\tau_2), \tag{20}$$

$$\chi_{\varphi/x}^{-1} = \frac{1}{4U} \delta(\tau_1 - \tau_2) \pm \frac{1}{8} \mathrm{Tr}\left[\boldsymbol{\alpha}_{\varphi/x} \mathbf{G}_0(\tau_1 - \tau_2) \boldsymbol{\alpha}_{\varphi/x} \mathbf{G}_0(\tau_2 - \tau_1) \right], \tag{21}$$

$$\mathbf{G}_0(\tau) = \left(a_0(\tau)\mathbf{1} + \frac{1}{2}(\bar{\varphi}\boldsymbol{\sigma}_z + \bar{x}\mathbf{1}) \delta(\tau) \right)^{-1}, \tag{22}$$

with $\boldsymbol{\alpha}_\varphi = \boldsymbol{\sigma}_z$ and $\boldsymbol{\alpha}_x = \mathbf{1}$ 2×2 matrices acting on spin space. In the mean-field approximation, a critical U exists; for $U < U_c, \bar{\varphi} = 0$, and for $U > U_c, \bar{\varphi} \neq 0$. (This transition is removed by fluctuations.) For $U \gtrsim U_c$, spin fluctuations are very soft.

We focus here on the φ integral, and we consider the small-U regime in which $\bar{\varphi} = 0$, and in the paramagnetic phase, where the x and φ integrals decouple. The mean square value of the fluctuations of $\varphi, \langle \varphi^2 \rangle$ (obtained by performing the Gaussian integral over all Matsubara components of φ), and the classical approximation $\langle \varphi^2 \rangle_{class}$ (obtained by performing the integral only over zero Matsubara components of φ) are

$$\langle \varphi^2 \rangle = -T \sum_l \frac{U^2 \chi_0(i\nu_l)}{1 + U\chi_0(i\nu_l)}, \tag{23}$$

$$\langle \varphi^2 \rangle_{class} = -T \frac{U^2 \chi_0(0)}{1 + U\chi_0(0)}, \tag{24}$$

where χ_0 is an irreducible susceptibility given by

$$\chi_0(i\nu_l) = 2T \sum_n a_0^{-1}(i\omega_n + i\nu_l) a_0^{-1}(i\omega_n), \tag{25}$$

with ν_l with ν_l being a bosonic Matsubara frequency. Finally, the leading perturbative contribution to the electron self-energy Σ and its classical approximation Σ_{class} are given by

$$\Sigma(i\omega_n) = \frac{1}{4} T \sum_l \chi(i\nu_l) a_0^{-1}(i\omega_n - i\nu_l), \tag{26}$$

$$\Sigma_{class}(i\omega_n) = \frac{1}{4} T \chi(0) a_0^{-1}(i\omega_n), \tag{27}$$

with the susceptibility

$$\chi(i\nu_l) = \frac{U^2 \chi_0(i\nu_l)}{1 + U\chi_0(i\nu_l)}. \tag{28}$$

We now present results obtained by applying the Gaussian approximation to the paramagnetic phase of the infinite-dimensional fcc lattice [the DOS is given by Eq. (3)]. In this section, energy is scaled by the variance of the DOS ($v=1$). The lower band edge is at $\varepsilon_{min} = -1/\sqrt{2} \approx -0.71$ and the square root divergence of the density of states means that for small fillings the density of states is very close to the bottom of the band. In the noninteracting limit the chemical potential is $\mu_{n=0.5} \approx -0.6335 (\mu - \varepsilon_{min} \approx 0.078)$ and $\mu_{n=0.75} = -0.5352 (\mu - \varepsilon_{min} \approx 0.175)$. The square root divergences mean that the critical interaction strengths beyond which the mean-field solution becomes unstable are themselves temperature dependent, and are small.

Figure 5 gives the comparison of the full Gaussian [Eq. (23)] and classical Gaussian fluctuation [Eq. (24)] approximations to the mean square fluctuation of the spin Hubbard-Stratonovich field for the infinite-dimensional fcc lattice model [Eq. (3)] with $n=0.5$ and 0.75. One sees that the classical approximation captures most of the fluctuations either for U near the critical value or for temperatures of the order of the bandwidth. The panels of Fig. 6 show the full Gaussian self-energy [Eq. (26)] and the classical Gaussian approximation [Eq. (27)] for different interaction values, for $n=0.75$. For small U, the semiclassical approximation fails, but as U approaches the critical value (here approximately 0.84) the self-energy becomes well represented by its classical approximation

The panels of Fig. 7 show the dependence of the self-energy on temperature, at a fixed moderate interaction strength (about 3/4 of the critical value). We see that at all temperatures studied, the classical Gaussian approximation [Eq. (27)] provides a reasonable estimate of the low-frequency self-energy. At temperatures less than about half of the bandwidth, the classical approximation grossly underestimates the high-frequency part of the self-energy, but by $T=0.08$ it is within about 30% of the exact value, and for higher temperatures or for interactions close to the critical value the approximation is quite good.

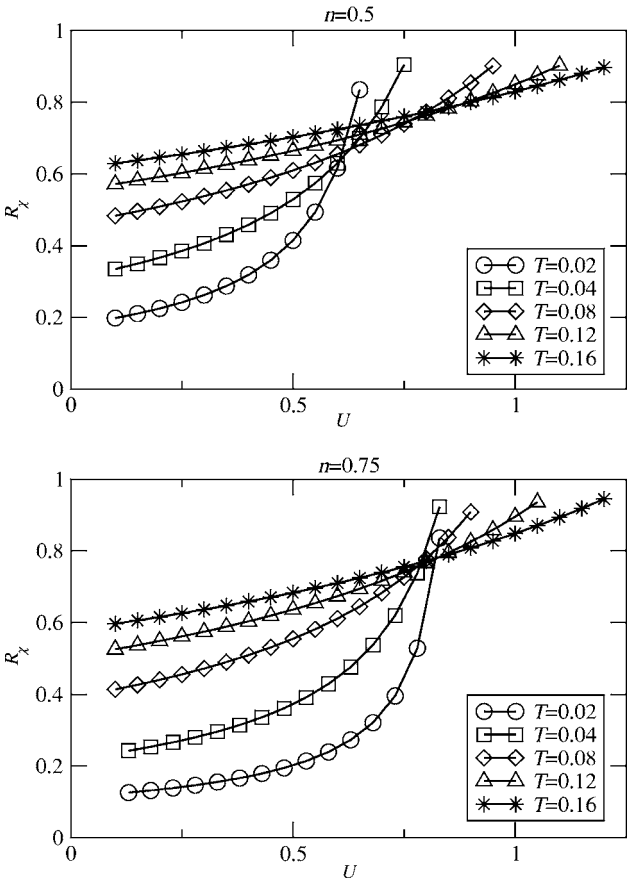

FIG. 5. Ratio of the classical Gaussian approximation [Eq. (24)] to the full Gaussian [Eq. (23)] mean square fluctuation of the spin Hubbard-Stratonovich field $R_\chi = \langle \varphi^2 \rangle_{class} / \langle \varphi^2 \rangle$ for infinite-dimensional fcc lattice at densities $n=0.5$ (upper panel) and 0.75 (lower panel). Energy is scaled by the variance of the free DOS ($v=1$). The curves cross because of the temperature dependence of the critical interaction strength (evident from the U at which the ratio approaches unity).

IV. COMPARISON OF SEMICLASSICAL APPROXIMATION TO QMC RESULTS: TWO-DIMENSIONAL SQUARE LATTICE

The Hubbard model on a bipartite lattice is known to exhibit an antiferromagnetic Néel ordering at half filling and finite U. In this section, we apply the semiclassical approximation to the Hubbard model with a square lattice [noninteracting electron dispersion is given by Eq. (1)], and investigate the self-energy, density of states, and magnetic transition temperature. Note that the finite T_N in a two-dimensional square lattice is an artifact arising from the neglect of the low-lying spin-wave excitation which the DMFT method cannot capture.

These results are compared with QMC calculations performed on computing facilities at Universität Bonn using the

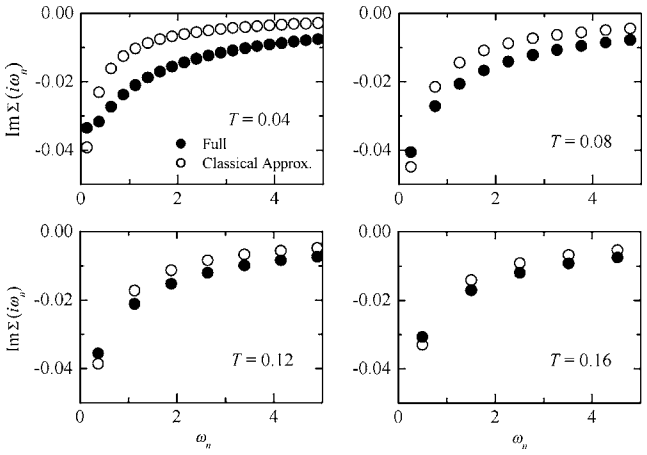

FIG. 6. Frequency dependence of full Gaussian self-energy [Eq. (26)] (filled circles) and classical Gaussian approximation [Eq. (27)] (open circles), for infinite-dimensional fcc lattice with $n=0.75, T=0.04$, and U values indicated. Energy is scaled by the variance of the free DOS ($v=1$).

Hirsch-Fye algorithm.[4] Typically, 48 time slices were used, and $(2-20)\times 10^6$ MC configurations were recorded. Occasional runs with more time slices or more MC configurations were made to verify error. Between five and (for the largest U) 25 iterations were needed for convergence of the DMFT loops. The Néel temperatures were determined from computations of the staggered magnetization. For $U \gtrsim 8t$ and T in or near the magnetic phase boundary, global update techniques (to be described elsewhere) were needed to ensure equilibration of the MC calculation. Error bars are smaller than the symbols shown.

As noted in the previous section, it is expected that the semiclassical approximation becomes accurate in the strong coupling regime and at high temperature. In order to confirm this expectation beyond the harmonic (Gaussian fluctuation) approximation, we first calculate the electronic self-energies in the paramagnetic state and compare them to the QMC

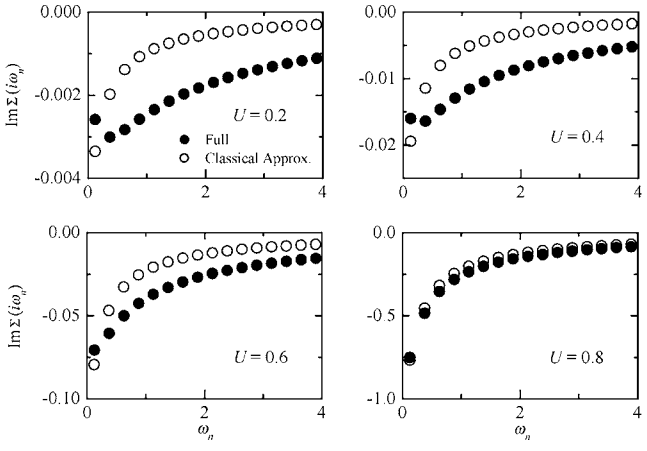

FIG. 7. Frequency dependence of imaginary part of full Gaussian self-energy [Eq. (26)] (filled circles) and classical Gaussian approximation [Eq. (27)] (open circles) for $n=0.75, U=0.5$, and T values indicated. Energy is scaled by the variance of the free DOS ($v=1$).

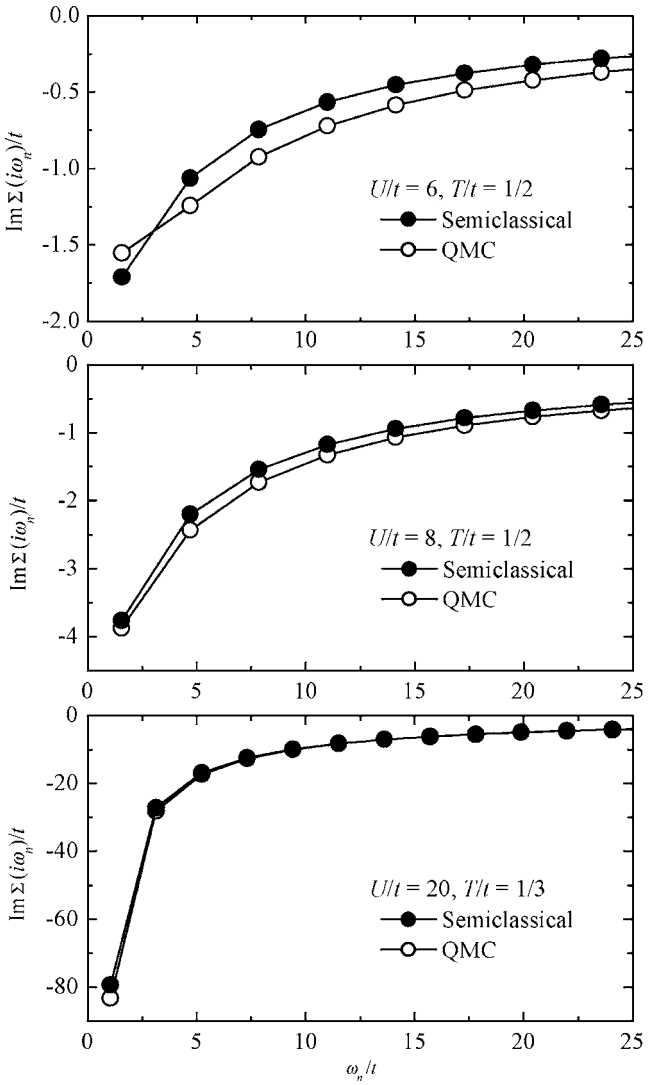

FIG. 8. Self-energies for a square-lattice half-filled Hubbard model computed from the semiclassical approximation (filled circles) and QMC calculations (open circles) for interactions and temperatures indicated.

results. Recall that for this model the full bandwidth is $8t$. In Fig. 8, shown are the self-energies at $U/t=6$ and $T/t=1/2$ (top panel), $U/t=8$ and $T/t=1/2$ (middle panel), and $U/t=20$ and $T/t=1/3$ (bottom panel) computed by the semiclassical approximation and QMC simulation as functions of imaginary frequency. With increase of U, the self-energy at low frequency increases and for $U>U_c$ diverges, indicating the Mott metal-insulator transition. This behavior is well reproduced by the semiclassical approximation, and the agreement with the QMC results is remarkable, particularly in the strong coupling regime.

Figure 9 compares the semiclassical results for a real-frequency quantity, the density of states, to results obtained by maximum entropy analytical continuation of the QMC data. This is a rather stringent test of the method, and agreement is seen to be reasonably good. In the weak coupling, paramagnetic phase [Fig. 9(a)], the semiclassical approximation underestimates the $\omega=0$ peak (because the $\omega=0$ scattering rate is overestimated) and underestimates the weight in

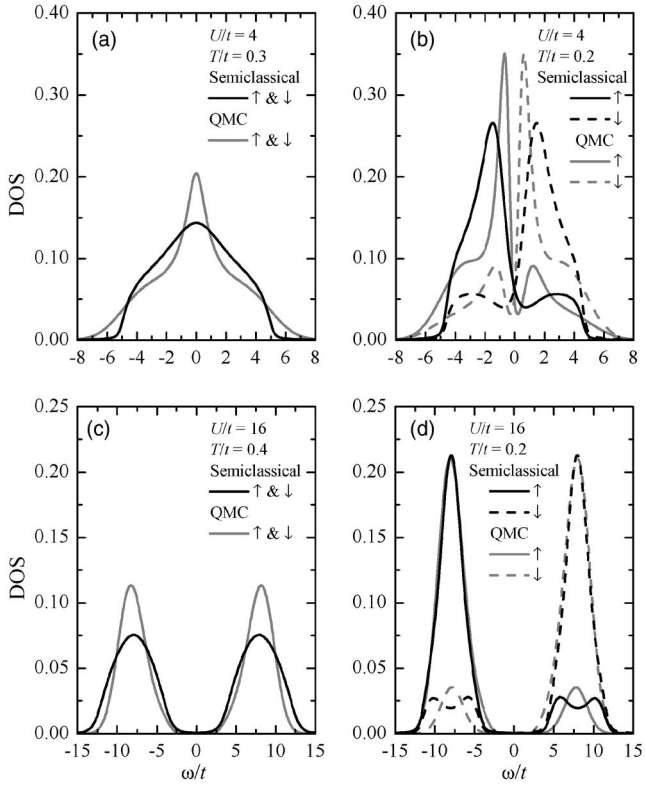

FIG. 9. Density of states of square-lattice half-filled Hubbard model computed using semiclassical (heavy lines) and QMC methods (light lines) for paramagnetic [(a) and (c)] and antiferromagnetic [(b) and (d), $T\sim 0.8T_N$] phases at interactions and temperatures indicated. In the antiferromagnetic phase, the majority spin density of states is shown by a solid line, the minority spin by a broken line.

the wings (because the high-frequency scattering rate is underestimated; see the upper panel of Fig. 8). Below T_N, the magnetization is slightly overestimated by the semiclassical approximation (magnetization $\langle m\rangle\sim 0.54$ for the semiclassical approximation and $\langle m\rangle\sim 0.4$ for QMC simulation at $U/t=4$ and $T/t=0.2$) as can be seen from the slightly larger gap. The DOS is sharper because the self-energy at high frequency is underestimated as in the paramagnetic state. In the strong coupling regime, agreement between the semiclassical approximation and the QMC simulation is quite good as can be expected from the self-energy (see the lower panel of Fig. 8).

Figure 10 summarizes results for the magnetic phase diagram obtained from the semiclassical approximation, QMC simulation, the HF approximation, and a strong coupling expansion. The semiclassical approximation is seen to give remarkably good results over the whole phase diagram. In the weak coupling limit, the semiclassical approximation gives correct behavior: T_N asymptotes to the result of the HF approximation in the limit of $U\rightarrow 0$. This is natural because the two approximations become identical in the $U\rightarrow 0, T\rightarrow 0$ limit. For U nonzero but small, the reduction of T_N from the HF value is found to be quite large, because the finite self-energy reduces nesting effects substantially. The present approximation gives correct behavior in the strong coupling

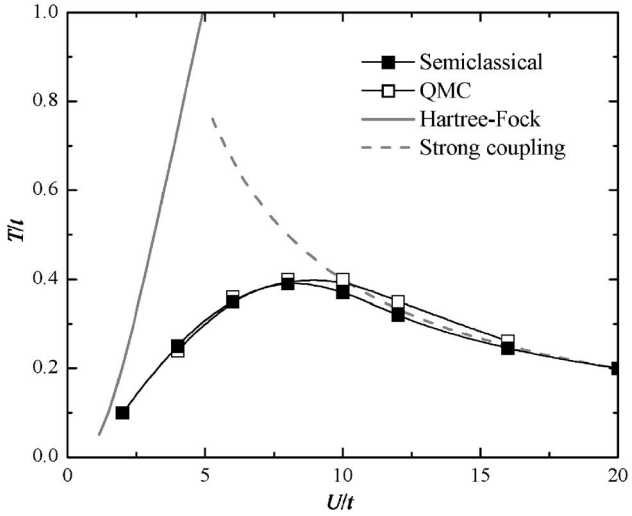

FIG. 10. Néel temperature of square-lattice half-filled Hubbard model as functions of U computed from semiclassical approximation (filled symbols) and QMC simulation (open symbols), HF (light solid line), and large-U limit ($T_N=4t^2/U$) (light broken line).

regime; T_N asymptotes to $4t^2/U$, the mean-field result of the strong coupling expansion, and, in particular, is almost identical to the QMC results. It should be noted that at large U and low T, the QMC simulation requires a very large amount of Monte Carlo sampling to reach equilibrium, whereas the semiclassical method is numerically very cheap. Even for $U/t=16$ and $T/t\sim 0.2$ (antiferromagnetic phase), it takes less than 5 min on a commercial PC to compute one point in the present method, while it takes ~6 h by QMC simulation on a similar computer for the same parameters.

V. COMPARISON OF SEMICLASSICAL APPROXIMATION TO QMC: FCC LATTICE

In this section, we apply the semiclassical approximation to the single-band Hubbard model on the fcc lattice in infinite and three dimensions, and compare the results to QMC data of Ulmke[43] and the "two-site" approximation of Potthoff.[25] We focus on the filling dependence of the magnetism in these models, in which the charge fluctuation plays an important role. At noninteger filling, these models order ferromagnetically because of the large DOS near the bottom of the band, in contrast to the antiferromagnetic ordering found in a half-filled square lattice. In addition, near half filling, the three-dimensional model is found to show an additional competing order: a "layer-type antiferromagnetic" state. We examine whether the semiclassical approximation captures this behavior. In this section, we use the variance of the DOS v as a unit of energy.

First, we apply the semiclassical approximation to the infinite-dimensional fcc lattice with DOS given in Eq. (3), $v=1$. The density of states above the Curie temperature is essentially the same as seen as the solid line in Fig. 3, and consists of two structures: one peak just below the Fermi level $\omega=0$ and a shoulder at $\omega\sim nU$. These correspond to the lower and upper Hubbard bands. (Note that the result shown

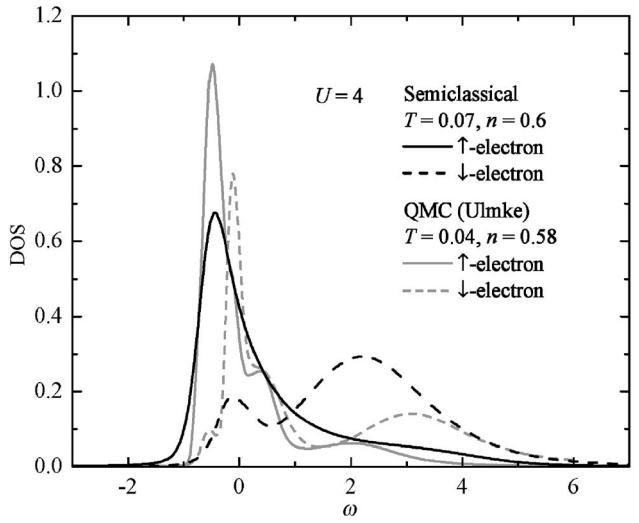

FIG. 11. Comparison of the density of states of infinite-dimensional FCC Hubbard model with $U=4$ and temperatures chosen so that $\langle m\rangle=0.4$ in each case. Energy is scaled by the variance of free DOS ($v=1$). Heavy lines: results of the semiclassical approximation at $n=0.6$ and $T=0.07$ ($\sim$13% below $T_C\sim 0.08$). Light lines: results of QMC at $n=0.58$ and $T=0.04$ ($\sim$20% below $T_C \sim 0.05$) taken from Ref. 43. Solid and broken lines are for the majority and minority spin.

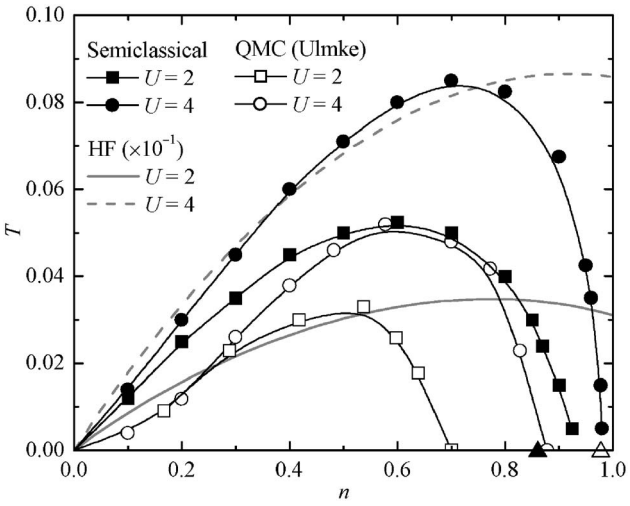

FIG. 12. Ferromagnetic Curie temperature of single-band Hubbard model on an infinite-dimensional fcc lattice as a function of electron density for $U=2$ (squares) and 4 (circles). Energy is scaled by the variance of the free DOS ($v=1$). Filled symbols, semiclassical approximation; open symbols, QMC simulation (Ref. 43). Curie temperatures ($\times 10^{-1}$) computed by HF approximation to the same model with $U=2$ (4) are shown as a light solid (broken) line. Two-site DMFT results for the transition temperatures are not shown, but representative two-site results for $n=0.5$ are $T_C \sim 0.17$ (0.26) for $U=2$ (4). Phase boundary at $T=0$ for $U=2$ (4) computed by the two-site DMFT is shown as a filled (open) triangle.

in Fig. 3 is computed at $T<T_C$, but in the paramagnetic phase, by suppressing the magnetic transition.) The separation between the lower and upper Hubbard bands is somewhat reduced from the bare value of U (by about a factor of the mean occupation number n), possibly because of the neglect of the fluctuation of the charge field. The two structures continuously evolve into the majority spin and minority spin bands below T_C as shown in Fig. 11.

Figure 11 also presents the DOS from a QMC simulation. (Temperature and density are chosen so that the magnetization in the two calculations is similar.) In QMC results, we observe a sharp peak below the Fermi level for the majority spin band. For the minority spin band, there appears a sharp peak near the Fermi level and a broad hump at $\omega\sim 3$. The former originates from the fact that the system is not fully polarized, and the latter corresponds to the upper Hubbard band. As noted above, the upper Hubbard band (broad hump around $\omega=3$ in the minority spin band) appears slightly low in energy in the semiclassical approximation. Except for this discrepancy, the overall structure of the DOS is well reproduced by the semiclassical approximation. In particular, the occupied bands below $\omega=0$ show reasonable agreement.

In Fig. 12, the ferromagnetic Curie temperatures T_C for different values of U are shown as functions of electron density. Filled symbols are the results obtained using the semiclassical approximation. For comparison, results of QMC simulations[43] and the HF approximation are shown as open symbols and light lines, respectively (note that the HF T_C values shown are reduced by a factor of 10). The semiclassical approximation overestimates T_C compared with QMC results by a factor of 1.5 over a wide range of density. (Of course, the difference near the critical density of the QMC method is much larger.) It is seen that the HF approximation is very poor in all parameter regimes, highly overestimating the ferromagnetic Curie temperature. The critical density n_c is also overestimated, at $n_c\sim 1.2$ at $U=2$ and $n_c\sim 1.5$ at $U=4$. The higher T_C found in the semiclassical approximation may be due to the neglect of the quantum fluctuation of the HS fields. The reduction of the transition temperature due to the quantum fluctuation can be seen in the context of electron-phonon coupling in Ref. 44. However, good agreement between the semiclassical approximation and QMC simulation indicates that the thermal part of the fluctuation dominates the electron self-energy in a wide region and, thus, the magnetic transition. Critical densities n_c where the ferromagnetism disappears at $T=0$ are found to be slightly higher in the semiclassical approximation than in QMC simulations, $n_c\sim 0.88$ for $U=2$ and $n_c\sim 0.97$ for $U=4$, while QMC simulation gives $n_c\sim 0.7$ for $U=2$ and $n_c\sim 0.88$ for $U=4$. However, in the light of the simplification of the present approximation, the agreement with QMC results within 20% error is remarkable.

We applied the two-site[25] DMFT to the same model to investigate the magnetic phase diagram. The critical densities n_c obtained by two-site DMFT are found to be very similar to those by the semiclassical approximation. However, Curie temperatures are found to be overestimated by a factor of ~ 6 compared with QMC simulation, and by a factor of $\sim$3–4 compared with the semiclassical approximation. In the two-site DMFT, T_C at $n=0.5$ is found to be ~ 0.17 for $U=2$, and ~ 0.26 for $U=4$. The overestimate arises because, in the two-site DMFT, the IAM is composed of only two sites; one is correlated (impurity) and one is noncorrelated (bath). The

energy difference between the eigenstates of the IAM is generically large, so the (spin) entropy is underestimated. The two-site DMFT also yields reentrant behavior near the critical concentration, which is not observed in the semiclassical approximation and QMC. Adding more sites in the "bath" part of the IAM would remedy these behaviors, but at drastically increased computational expense.

Finally, we investigate the magnetic instability in the more realistic three-dimensional fcc lattice whose free band dispersion is given in Eq. (2). Following Ref. 43, we take $t'=t/4$ and choose the variance of the DOS $v=\sqrt{12t^2+6t'^2}$ as the energy unit; thus $t\approx 0.284$ and $t'\approx 0.071$. With this parameter set, the bottom of the band is given by $\varepsilon_{min}=-4t+2t'\approx -0.994$. There is no divergence in the free DOS in contrast to the infinite-dimensional case.

The magnetic phase diagram of the three-dimensional fcc lattice computed by the semiclassical approximation is shown in Fig. 13. For comparison, QMC (Ref. 43) and HF results are also plotted. It is seen that the semiclassical-approximation results for T_C are about twice higher than QMC results, while HF results are about 20 times higher than QMC results. Similar to the infinite-dimensional case, the upper critical density n_c is overestimated by $\sim 20\%$. QMC calculations are argued to indicate that there exists a lower critical density $n_c'\sim 0.15$ below which the ferromagnetism disappears.[43] This behavior is ascribed to the absence of the divergence at the bottom of the bare DOS. In the semiclassical approximation, T_C seems to become zero proportionally to the electron density, similarly to the HF approximation. In the latter, clearly $n_c'=0$. This might be because the semiclassical approximation reduces to the HF result at weak coupling (in this case small density) and in the low-temperature limit. However, it is very difficult to judge if $n_c'=0$ or not in the present accuracy for the semiclassical approximation.

Differently from the infinite-dimensional fcc lattice, the QMC calculation found another magnetic state stabilized near $n=1$: a layer-type antiferromagnetic state with a magnetic vector $\vec{q}=(\pi,0,0)$.[43] The semiclassical approximation is successful in finding the layer-type antiferromagnetic state near $n=1$. The computed Néel temperature at $n=1$ is $T_N\sim 0.048$ which agrees with the QMC result within the statistical error of the QMC simulation. The better agreement in the Néel temperature than in the Curie temperature may be attributed to the large U used in this calculation and to the suppression of the charge fluctuations near half filling. According to the two-site DMFT, the critical U_c to the Mott transition at half filling is estimated to be $U_c=6v$ (the correct value is expected to be slightly smaller then this).[25] With the parameter used, $U=6$, the system is in a Mott insulating state at $n=1$, and the charge fluctuation is suppressed. Therefore, the thermal fluctuation of the spin field dominates the magnetic transition. In contrast to the QMC simulation, ferromagnetic and antiferromagnetic states contact with each other in the semiclassical approximation. (In the semiclassical result, T_C and T_N indicate the instability of the ferromagnetic and antiferromagnetic states, respectively, to the paramagnetic state.) In light of the overestimation of the upper critical density n_c for the ferromagnetism, this failure is also supposed to be from the neglect of the quantum fluctuation of the HS field. This point remains to be addressed in future work.

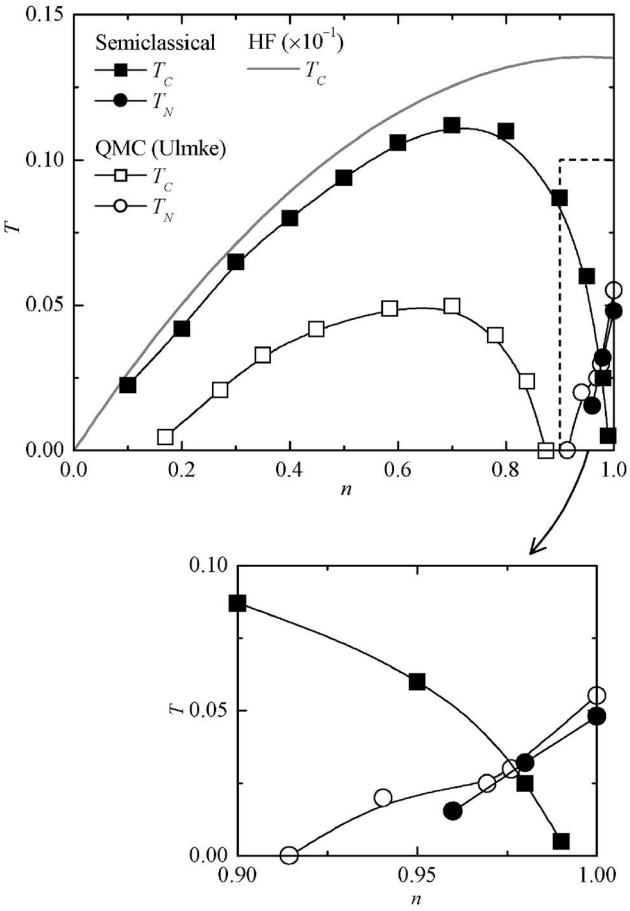

FIG. 13. Upper panel: Phase diagram of single-band Hubbard model on a three-dimensional fcc lattice as a function of electron density and temperature for interaction $U=6$. Energy is scaled by the variance of the free DOS ($v=1$). Squares and circles are the Curie temperature and Néel temperature for the layer-type antiferromagnetic state, respectively. Filled symbols, results of the semiclassical approximation; open symbols, QMC results taken from Ref. 43. Curie temperature ($\times 10^{-1}$) computed by HF approximation to the same model is shown as a light solid line. Lower panel: Expansion of the phase diagram, showing the region near $n=1$ enclosed by a broken line in the upper panel. The semiclassical results for T_C and T_N indicate the instability of ferromagnetic and antiferromagnetic states, respectively, toward the paramagnetic state.

In the metallic region, one needs to fix the chemical potential according to the density—this must be done at each interaction strength and temperature, which is time consuming. Even in this case, the semiclassical scheme is found to be computationally very cheap. Typical CPU time is less than 5 min at $U=2$ and $T=0.05$ using a commercial PC.

Summarizing this section, we investigated the magnetic behavior of the Hubbard model on infinite- and three-dimensional fcc lattices using the semiclassical approximation. The magnetic phase diagram computed by the semiclassical approximation show reasonable agreement with QMC results. The ferromagnetic Curie temperature in the metallic region is found to be within a factor of ~ 2 compared with the QMC result, and the antiferromagnetic Néel temperature

near $n=1$ is found to agree with the QMC value within statistical error. The better agreement between the semiclassical approximation and QMC simulation in the Néel temperature near integer filling is supposed to be from the fact that the charge fluctuation is suppressed by the correlation, so that thermal spin fluctuations dominate the transition as in the half-filled square-lattice case. The poorer agreement in the Curie temperature is expected to be from the neglect of quantum fluctuation or charge fluctuation.

VI. APPLICATION OF SEMICLASSICAL APPROXIMATION TO THE DYNAMICAL CLUSTER APPROXIMATION AND FICTIVE-IMPURITY METHOD

Our semiclassical approximation is easily combined with cluster schemes, such as the dynamical cluster approximation[47] (DCA) and real-site cluster extension of DMFT.[40,48,49] As a simplest example, we use the two-site DCA and fictive-impurity[40] (FI) methods to study the Hubbard model on a square lattice.

We consider half filling; thus charge fields are absorbed into the chemical potential shift. The Weiss field becomes a 2×2 matrix $\mathbf{a}$, and in the paramagnetic phase this takes the form

$$\mathbf{a} = a_0 \mathbf{1} + a_1 \boldsymbol{\tau}_x, \tag{29}$$

with a_0 and a_1 being the on-site and NN Weiss fields, respectively. $\mathbf{1}$ and $\boldsymbol{\tau}_x$ are the 2×2 matrices acting on orbital (impurity site) space. The HS transformation is performed at each impurity site $i=1$, 2 with spin field φ_i. The effective potential for the HS field becomes

$$V(\varphi_1,\varphi_2) = \frac{1}{4U}(\varphi_1^2+\varphi_2^2) - T\,\mathrm{Tr}\,\ln\left[-\mathbf{a} - \frac{1}{2}\begin{pmatrix}\varphi_1 & \\ & \varphi_2\end{pmatrix}\boldsymbol{\sigma}_z\right]. \tag{30}$$

Here, $\boldsymbol{\sigma}_z$ is acting on spin space, and Tr is taken over the Matsubara frequency and orbital and spin indices. Then, the partition function is given as

$$Z_{approx} = \int d\varphi_1 d\varphi_2 \exp\{-\beta V(\varphi_1,\varphi_2)\}. \tag{31}$$

Finally, on-site and NN-site Green's functions G_0 and G_1, respectively, are obtained via

$$G_0 = \frac{1}{2}\frac{\delta \ln Z_{approx}}{\delta a_0}, \tag{32}$$

$$G_1 = \frac{1}{2}\frac{\delta \ln Z_{approx}}{\delta a_1}. \tag{33}$$

The self-consistency equations for the DCA are closed following the scheme presented in Ref. 47. The self-consistency equations for the FI method and the general formalism for the cluster extension of DMFT are given in Ref. 40.

Nearest-neighbor spin correlations $-\langle\sigma_{1z}\sigma_{2z}\rangle$ computed by the DCA and FI with the semiclassical approximation and QMC simulation as functions of temperature for $U=20t$ are shown in Fig. 14. A similar spin correlation obtained by QMC simulation in both the DCA and FI supports the applicability of the semiclassical approximation to the cluster DMFT. For comparison, the same quantity computed using a high-temperature series expansion (HTS) for the $S=1/2$ NN Heisenberg model with $J=t^2/U$ is also shown. It is seen that the spin correlation obtained from the DCA is much larger than the HTS result. We believe the origin of the discrepancy between DCA and HTS is that the DCA is equivalent to imposing a periodic boundary condition in all the directions in a real-space cluster. Thus, in the two-site DCA, one has a model in which two sites are connected via z bonds (connectivity $z=4$ in a square lattice) and the spin correlation is thus overestimated. Interestingly, the FI method gives almost identical curves to the HTS (a slight deviation can be seen below $T\sim 0.4t$). A detailed study of multisite cluster models using semiclassical methods and QMC simulation will be presented elsewhere.[50]

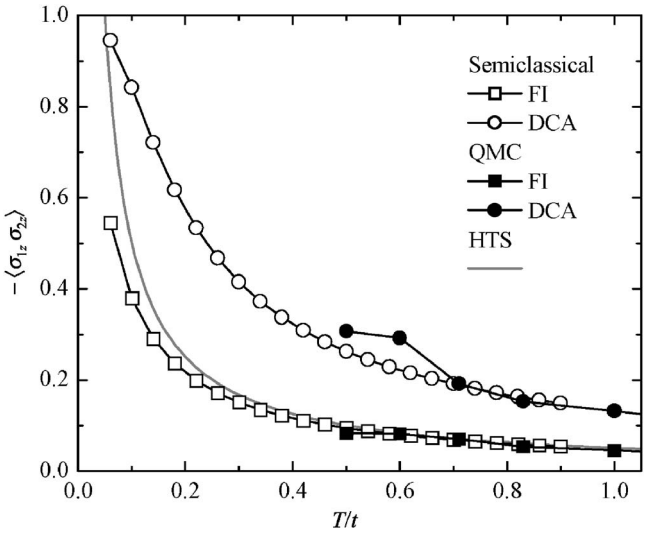

FIG. 14. Nearest-neighbor spin correlations $-\langle\sigma_{1z}\sigma_{2z}\rangle$ of a square-lattice Hubbard model ($U/t=20$) as functions of T computed using two-site DCA (open circles) and the FI method (open squares), compared to QMC simulation (filled symbols) and high-temperature series expansion (light line).

VII. EQUILIBRATION AND PARTITIONED PHASE SPACE

In this section, we point out an additional advantage of the semiclassical approximation. A key issue in Monte Carlo simulations is equilibration, which is particularly difficult in systems in which the phase space is partitioned into several nearly equivalent minima, separated by large barriers. Local update techniques require extremely long runs to climb over barriers, while global update techniques are expensive and sometimes inconvenient to implement and bring their own convergence issues. The partitioned phase space phenomenon occurs frequently in strongly correlated models, and represents a significant obstacle to practical computations. The semiclassical approximation, by contrast, is inexpensive enough that the entire (semiclassical) phase space can be sampled.

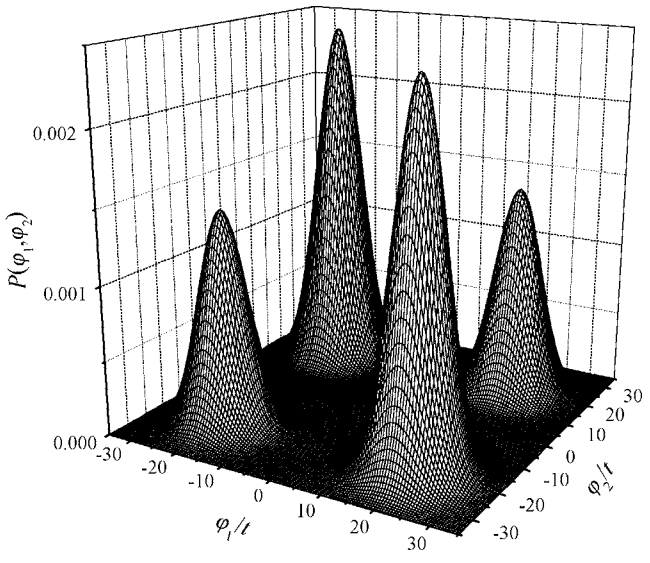

FIG. 15. Distribution of the spin fields φ_1 and $\varphi_2, P(\varphi_1, \varphi_2)$, computed by the two-impurity DCA for the Hubbard model on a square lattice. $P(\varphi_1, \varphi_2)$ is defined by $P(\varphi_1, \varphi_2) = \exp\{-\beta V(\varphi_1, \varphi_2)\}/Z_{approx}$. Parameters are $U/t=20$ and $T/t=0.5$. Larger peaks at $(\varphi_1, \varphi_2) \simeq (\pm 20t, \mp 20t)$ than at $(\varphi_1, \varphi_2) \simeq (\pm 20t, \pm 20t)$ indicate antiferromagnetic correlation.

For example, Fig. 15 shows the distribution function of spin HS fields for the two-impurity DCA for the square-lattice half-filled Hubbard model defined by $P(\varphi_1, \varphi_2) = \exp\{-\beta V(\varphi_1, \varphi_2)\}/Z_{approx}$ computed at temperature $T/t = 0.5 > T_N$ (see Fig. 10). The partitioning of phase space is evident. It is seen that the distribution has twofold symmetry, not fourfold, in the $\varphi_1 - \varphi_2$ plane; $\varphi_1 > \varphi_2$ and $\varphi_1 < \varphi_2$ are not equivalent. Larger peaks at $(\varphi_1, \varphi_2) \simeq (\pm 20t, \mp 20t)$ than at $(\varphi_1, \varphi_2) \simeq (\pm 20t, \pm 20t)$ indicate that the antiferromagnetic correlations prevail far above the Néel temperature, giving the result shown in Fig. 14. Reliable estimates of $-\langle \sigma_{1z} \sigma_{2z} \rangle$ require sampling of all four extremes, with correct weights, which is very difficult to achieve in QMC simulations at low T (this is why we do not present data at $T < 0.5t$, and statistical errors are evident even at $T=0.6t$). However, the integrals involved in the semiclassical method may be performed with no difficulty.

VIII. SUMMARY AND DISCUSSION

In this paper, we investigated the semiclassical approximation to the continuous Hubbard-Stratonovich transformation as an impurity solver of the DMFT method for correlated-electron models. The Hubbard-Stratonovich transformation introduces two auxiliary fields, coupling to the electron spin and charge density, respectively. The semiclassical approximation consists of retaining only the classical (zero-Matsubara-frequency) component in the functional integral over the spin field, and, for each value of the spin field, using a steepest descent approximation to approximate the integral over the charge field by the value that minimizes the action at the given value of the spin field [see Eq. (15)]. This treatment of the charge field was found to be essential for achieving reasonable results: see Fig. 3 and the associated discussion. The semiclassical approximation captures the thermal fluctuation of spin field efficiently beyond the harmonic (Gaussian fluctuation) approximation and is applicable to both the metallic and insulating regions. Estimates obtained using the Gaussian fluctuation approximation indicate that the semiclassical approximation gives reasonable results at larger U (when spin fluctuations are soft) or at high temperature (Sec. III). We applied the semiclassical approximation to the single-band Hubbard model on a two-dimensional square lattice (half filling) (Sec. IV) and infinite- and three-dimensional fcc lattices (finite doping) (Sec. V). The semiclassical approximation is found to give reasonable results, with accuracy improving for stronger couplings and in situations where charge fluctuations are suppressed. A particularly attractive finding is that the procedure finds multiple phases when these exist (Fig. 13). The key point appears to be that, at stronger correlations, the physically important fluctuations become very soft (justifying a semiclassical approximation) but very anharmonic (requiring an integral over all field configurations). Due to the neglect of quantum effects, the semiclassical approximation fails to reproduce correctly the quasiparticle resonance, which will certainly be important at weak coupling or at low temperature. One possible improvement of this failure would be by using an interpolative method[29] to reproduce the low-energy quasiparticle in a paramagnetic metallic region. For the half-filled square lattice, we showed that the semiclassical approximation gives reasonable behavior of the self-energy which is comparable to QMC simulation in a wide range of parameters. The density of states and Néel temperature computed by the semiclassical approximation are found to be in very good agreement with the QMC simulation. In the metallic fcc lattice, the DOS has a two-peak structure corresponding to the lower and upper Hubbard bands in a paramagnetic phase. These structures evolve into majority and minority spin bands as the temperature is decreased through the ferromagnetic transition. Comparison of the DOS computed by the semiclassical approximation and by QMC simulation shows reasonable agreement, especially as concerns the occupied state. Ferromagnetic Curie temperatures computed by the present method are found to be in the range of a factor of 2 compared with the QMC results. $T=0$ phase boundaries are found to be within the error of 20%. The semiclassical approximation for the Curie temperature shows better agreement than two-site DMFT, and $T=0$ phase boundaries are found to be in the same range as in the two-site DMFT. As for the three-dimensional fcc lattice, the semiclassical approximation is able to detect the antiferromagnetic state near the integer filling consistent with QMC computations. The Néel temperature in this case agrees with the QMC result within the statistical error. In Sec. VI, we apply the semiclassical approximation to the two-impurity DCA and real-space cluster DMFT (fictive impurity) for the square-lattice Hubbard model at half filling, and investigate how spatial correlation is taken into account in the present approximation. We confirmed that the short-range (nearest-neighbor) spin correlation prevails above the Néel temperature. Comparison of nearest-neighbor spin correlation between the semiclassical approximation and QMC simulation shows good agreement

in ranges where the QMC calculations are well converged. In Sec. VII, the equilibration problem in the QMC method associated with the partition of phases is discussed. This problem does not occur in the semiclassical approximation.

In conclusion, we mention some open scientific questions which can be addressed by the semiclassical method, and mention two areas in which further investigation and improvement would be desirable. A key opportunity involves systems with several sites and/or several orbitals. In such cases, QMC simulation suffers from "sign" problems, and both QMC and ED methods scale poorly with system size. The semiclassical method does not suffer from the "sign" problem; while there appeared a similar problem associated with the imaginary coefficient for the charge field, this is resolved by applying the saddle-point approximation to the charge field. When it is applied to systems with $N>1$ orbitals (on one or more sites), computational time for the semiclassical approximation scales of P_{φ}^{N} with P_{φ} and N being the total number of discretized HS field and total number of sites/orbitals, respectively. By contrast in Monte Carlo methods, the scaling is $[(\beta U)^2 N_{MC}]^N$ (N_{MC} is the number of Monte Carlo samplings, typically $N_{MC}\sim 10^5$), and by $4^{N(1+N_{bath})}$ for ED (N_{bath} is the number of "bath" sites per impurity orbital, and N_{bath} should be larger than 2–3 from the overestimation of T_C by two-site DMFT). As can be seen in Fig. 15, the dominant contribution is known to be from $|\varphi| \sim U$, and if needed it would be possible to simplify the N-dimensional integral over the HS fields. Thus, the semiclassical approximation appears to be an attractive option for studying larger clusters which are not accessible by QMC simulation.

As for the multisite problem, we have only applied the semiclassical approximation to the single-orbital Hubbard model at half filling with the DCA and FI method. In this case, the charge field is absorbed into the chemical potential. Away from half filling, one needs to fix the charge field at each configuration of the spin fields according to Eq. (15) generalized to the multisite situation. There is no proof that Eq. (15) has unique solution in this situation although we have so far not encountered problems. This issue needs further investigation.

As one of the applications of the semiclassical approximation, investigation of a systems with degenerate orbitals like transition-metal oxides with e_g or t_{2g} electrons would be interesting.[2,3] Theoretical studies of the ferromagnetism in these situations have been presented (Refs. 35–37), but these works dealt with spin fluctuations in the metallic state; fluctuation and ordering associated with the quadrupole moments for the e_g and/or t_{2g} orbital was neglected. The Hubbard-Stratonovich transformation including the spin and quadrupole moment for the two-band Hubbard interaction for the e_g orbital has been introduced in Ref. 38. However, spin and orbital transitions at finite temperature using the multiband Hubbard model with full symmetry[51] remain to be investigated.

Another promising application of the semiclassical approximation would be spatially inhomogeneous systems, where the computational expense associated with other aspects of the problem renders an inexpensive impurity solver essential. Recently, two of the authors (S.O. and A.J.M.) applied two-site DMFT to the spatially inhomogeneous heterostructure problem and investigated the evolution of the electronic state (quasiparticle band and upper and lower Hubbard bands) as a function of distance from the interface.[52] Applying the semiclassical approximation to such systems to investigate the possible spin (and orbital) orderings[53] is an interesting and urgent task.

ACKNOWLEDGMENTS

The authors acknowledge useful discussions with B. G. Kotliar and M. Potthoff. This research was supported by the JSPS (S.O.), DAAD, DFG-SFB 608 (A.F.), NSF Grant No. DMR 0431350 (A.C.), and the DOE under Grant No. ER 46169 (A.J.M.).

*Electronic address: okapon@phys.columbia.edu

[1] J. G. Bednorz and K. A. Muller, Z. Phys. B: Condens. Matter **64**, 189 (1986).
[2] M. Imada, A. Fujimori, and Y. Tokura, Rev. Mod. Phys. **70**, 1039 (1998).
[3] Y. Tokura and N. Nagaosa, Science **288**, 462 (2000).
[4] A. Georges, G. Kotliar, W. Krauth, and M. J. Rozenberg, Rev. Mod. Phys. **68**, 13 (1996).
[5] W. Metzner and D. Vollhardt, Phys. Rev. Lett. **62**, 324 (1989).
[6] A. Georges and G. Kotliar, Phys. Rev. B **45**, 6479 (1992).
[7] V. I. Anisimov, A. I. Poteryaev, M. A. Korotin, A. O. Anokhin, and G. Kotliar, J. Phys.: Condens. Matter **9**, 7359 (1997).
[8] S. Savrasov, G. Kotliar, and E. Abrahams, Nature (London) **410**, 793 (2001).
[9] K. Held, G. Keller, V. Eyert, D. Vollhardt, and V. I. Anisimov, Phys. Rev. Lett. **86**, 5345 (2001).
[10] X. Dai, S. Y. Savrasov, G. Kotliar, A. Migliori, H. Ledbetter, and E. Abrahams, Science **300**, 953 (2003).
[11] X. Y. Zhang, M. J. Rozenberg, and G. Kotliar, Phys. Rev. Lett. **70**, 1666 (1993).
[12] A. Georges and W. Krauth, Phys. Rev. B **48**, 7167 (1993).
[13] H. Kajueter and G. Kotliar, Phys. Rev. Lett. **77**, 131 (1996).
[14] Th. Pruschke, D. L. Cox, and M. Jarrell, Phys. Rev. B **47**, 3553 (1993).
[15] G. Moeller, Q. Si, G. Kotliar, M. Rozenberg, and D. S. Fisher, Phys. Rev. Lett. **74**, 2082 (1995).
[16] S. Florens, A. Georges, G. Kotliar, and O. Parcollet, Phys. Rev. B **66**, 205102 (2002).
[17] M. Jarrell, Phys. Rev. Lett. **69**, 168 (1992).
[18] M. J. Rozenberg, X. Y. Zhang, and G. Kotliar, Phys. Rev. Lett. **69**, 1236 (1992).
[19] A. Georges and W. Krauth, Phys. Rev. Lett. **69**, 1240 (1992).
[20] M. Caffarel and W. Krauth, Phys. Rev. Lett. **72**, 1545 (1994).
[21] O. Sakai and Y. Kuramoto, Solid State Commun. **89**, 307 (1994).
[22] R. Bulla, Phys. Rev. Lett. **83**, 136 (1999).
[23] D. J. Garcia, K. Hallberg, and M. J. Rozenberg, Phys. Rev. Lett.

93, 246403 (2004).
[24] S. Nishimoto, F. Gebhard, and E. Jeckelmann, J. Phys.: Condens. Matter **16**, 7063 (2004).
[25] M. Potthoff, Phys. Rev. B **64**, 165114 (2001).
[26] M. Potthoff, Eur. Phys. J. B **32**, 429 (2003).
[27] H. O. Jeschke and G. Kotliar, Phys. Rev. B **71**, 085103 (2005).
[28] J.-X. Zhu, R. C. Albers, and J. M. Wills, cond-mat/0409215 (unpublished).
[29] S. Y. Savrasov, V. Oudovenko, K. Haule, D. Villani, and G. Kotliar, Phys. Rev. B **71**, 115117 (2005).
[30] X. Dai and G. Kotliar, cond-mat/0412505 (unpublished).
[31] J. Hubbard, Phys. Rev. Lett. **3**, 77 (1959); R. L. Stratonovich, Dokl. Akad. Nauk SSSR **115**, 1097 (1958) [Sov. Phys. Dokl. **2**, 416 (1958)].
[32] H. Hasegawa, J. Phys. Soc. Jpn. **49**, 178 (1980); **49**, 963 (1980).
[33] S. Blawid and A. Millis, Phys. Rev. B **62**, 2424 (2000).
[34] S. Pankov, G. Kotliar, and Y. Motome, Phys. Rev. B **66**, 045117 (2002).
[35] I. S. Tyagi, R. Kishore, and S. K. Joshi, Phys. Rev. B **12**, 3809 (1975).
[36] H. Hasegawa, J. Phys. F: Met. Phys. **13**, 1915 (1983).
[37] Y. Kakehashi, Phys. Rev. B **34**, 3243 (1986).
[38] S. Ishihara, M. Yamanaka, and N. Nagaosa, Phys. Rev. B **56**, 686 (1997).
[39] P. Sun and G. Kotliar, Phys. Rev. B **66**, 085120 (2002).
[40] S. Okamoto, A. J. Millis, H. Monien, and A. Fuhrmann, Phys. Rev. B **68**, 195121 (2003).
[41] A. J. Millis, R. Mueller, and B. I. Shraiman, Phys. Rev. B **54**, 5389 (1996).
[42] E. Müller-Hartmann, in *Proceedings of the Fifth Symposium on Physics of Metals*, Ustroń, Poland, 1991, edited by E. Talik and J. Szade (unpublished), p. 22.
[43] M. Ulmke, Eur. Phys. J. B **1**, 301 (1998).
[44] S. Blawid and A. J. Millis, Phys. Rev. B **63**, 115114 (2001).
[45] H. Attias and Y. Alhassid, Nucl. Phys. A **625**, 565 (1997).
[46] S. Blawid, A. Deppeler, and A. J. Millis, Phys. Rev. B **67**, 165105 (2003).
[47] M. H. Hettler, A. N. Tahvildar-Zadeh, M. Jarrell, T. Pruschke, and H. R. Krishnamurthy, Phys. Rev. B **58**, R7475 (1998).
[48] G. Kotliar, S. Y. Savrasov, G. Palsson, and G. Biroli, Phys. Rev. Lett. **87**, 186401 (2001).
[49] G. Biroli and G. Kotliar, Phys. Rev. B **65**, 155112 (2002).
[50] A. Fuhrmann, S. Okamoto, and A. J. Millis (unpublished).
[51] T. Mizokawa and A. Fujimori, Phys. Rev. B **51**, R12880 (1995).
[52] S. Okamoto and A. J. Millis, Phys. Rev. B **70**, 241104(R) (2004).
[53] S. Okamoto and A. J. Millis, Nature (London) **428**, 630 (2004); Phys. Rev. B **70**, 075101 (2004).